Composites: Part A 173 (2023) 107659

Contents lists available at ScienceDirect

Composites Part A

journal homepage: www.elsevier.com/locate/compositesa

Formation of non-uniform fibre distributions in winding-pultrusion process and its effect on axial compressive properties of hollow GFRP profiles

Songming Qi [a], Omar Alajarmeh [a], Tristan Shelley [a], Peter Schubel [a], Kendric Rendle-Short [b], Xuesen Zeng [a,*]

[a] University of Southern Queensland, Centre for Future Materials, Toowoomba, Queensland 4350, Australia
[b] Wagners Composite Fibre Technologies, Wellcamp, Queensland 4350, Australia

ARTICLE INFO

Keywords:
B. Defects
B. Fibre deformation
B. Mechanical properties
D. Optical microscopy
E. Pultrusion

ABSTRACT

This study investigated the formation and impact of Non-Uniform Fibre Distribution (NUFD) in pultruded Glass Fibre Reinforced Polymer (GFRP) composite profiles. These profiles, manufactured through a pull-winding process, are low-cost, high-volume structure materials. NUFD, a result of defects such as fibre waviness, wrinkling and voids, lead to differences in fibre volume fraction through the profile cross-section. Image analysis was used to measure the NUFD, and its effect on the axial compressive behaviour was evaluated at both material and structural levels. Results show that material compressive strength has a maximum strength reduction of 11% observed in the tested material coupon. In long-column structural applications governed by local buckling failure mode, the finite element analysis highlights that the corner NUFD can lead up to a 9% reduction in axial compressive peak load due to the rotation stiffness variation when corner fibre content decreases by 30%.

1. Introduction

Fibre Reinforced Polymer (FRP) composites have been widely utilised in the aerospace, defence, infrastructure, and marine sectors due to their remarkable strength-to-weight ratio, resistance to corrosion and low life-cycle maintenance[1,2]. Despite their benefits, challenges remain in manufacturing defects such as fibre misalignment, voids, and fibre waviness, especially for complex shapes [3]. Imperfections in composite materials can significantly affect their compressive properties, making it crucial to quantify their impact on material strength and failure modes for designing and optimising composite structures [4].

Prior research on the Pultruded FRP (PFRP) composites has typically assumed that the unidirectional (UD) plies are uniform and defect-free [5]. However, the use of continuous strand mats (CSMs) or wound fibre plies results in Non-Uniform Fibre Distribution (NUFD). This phenomenon was noted from the cross-section of profiles and quantified by the variations in the local fibre volume fraction (Vf) [6–8]. The NUFD is always accompanied by resin-rich pockets, mat wrapping errors, cracks, and roving shifts, which affect mechanical properties [9–12]. The influence of geometric imperfections on structural performance related to local buckling is investigated through a nonlinear geometry model [13]. The relationship between fibre content and compressive failure strength has been studied using a normalised Vf at the material level [4]. However, no research systematically examines the formation of NUFD and its influence on compressive strength both at the material and structural levels.

Quantitative techniques have been applied to analyse the NUFD in various composite shapes, including manual plotting [6], calcination tests [7], X-ray micro-computed tomography [14–16], and optical microscopes [17]. Among the techniques above, microscopic methods have the advantage of being comparatively more straightforward and cost-effective. This research will focus on an image-based analysis to measure the UD fibre content of the profile cross-sections, quantifying the exact fibre distribution as input for the finite element (FE) analysis.

Pultrusion is a cost-effective method for producing composite profiles with uniform cross-sections that can operate continuously and autonomously [18–21]. The integration of the winding process in pultrusion enhances the lateral properties of PFRP composites through continuous-wound fibres [22,23]. Fig. 1(a) depicts a typical pull-winding production line, including the pull-winding fibre preforming and pultrusion systems. The first stage involves producing the dry fibre preforms, while the second stage is for resin infusion, consolidation/curing and cutting [24]. The mandrel in the preform section is often circular to improve winding stability. A transition section is used to

* Corresponding author.
E-mail address: xuesen.zeng@usq.edu.au (X. Zeng).

https://doi.org/10.1016/j.compositesa.2023.107659
Received 12 March 2023; Received in revised form 10 May 2023; Accepted 12 June 2023
Available online 16 June 2023

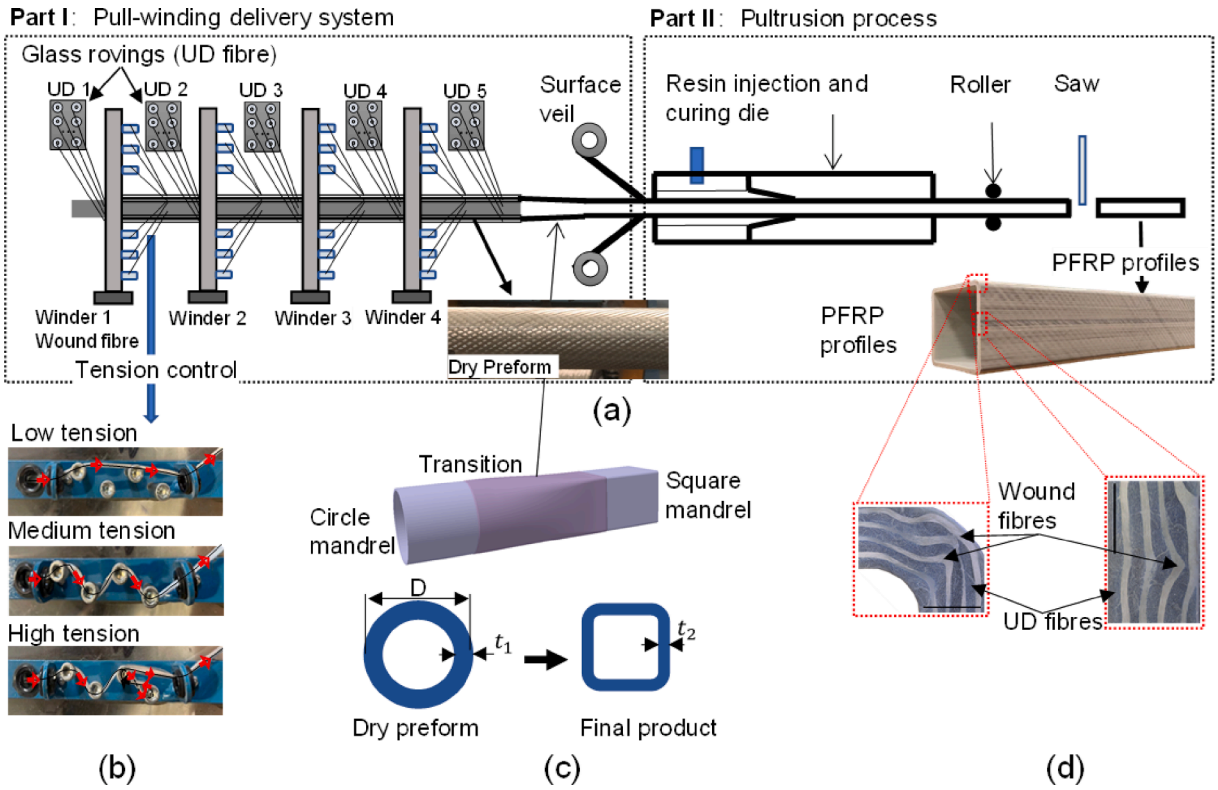

Fig. 1. (a) Illustration of pull-winding pultrusion process with a die-injection, (b) winding tension set up, (c) transition zone and thickness variation, and (d) typical non-uniform fibre distribution.

convert the cross-section based on equal circumferential perimeters for profiles with square or rectangular cross-sections, as shown in Fig. 1(c). In the final products, the wound fibres often exhibit numerous wrinkles, which are especially prevalent at the corners, and contribute to the formation of NUFDs, as shown in Fig. 1(d).

NUFD refers to the combined effects of in-plane waviness and out-of-plane waviness in composite materials. These waviness imperfections can cause the fibres to deviate from their intended alignment, leading to variations in fibre Vf and orientation within the material. Previous studies have described the mechanism of the waviness formation in the FRP composites through experiments [25–27] and numerical methods [28–30]. Waviness adversely affects mechanical performance, particularly compressive and tensile strength [31,32]. In addition, it can influence the initiation and propagation of damage [33]. In the case of pull-wound hollow FRP profiles, fibre waviness of the off-axis ply will interact with UD plies, resulting in fibre disturbance in the form of NUFD. The inter-ply interaction between fibre waviness and NUFD has not received much attention in prior publications. This research, therefore, will focus on the formation and influence of NUFD caused by waviness on the compressive strength of PFRP composite profiles.

In this research, NUFDs of varying levels were manufactured through pull-winding technology to examine the inter-ply relationship between fibre waviness and the NUFD. An image analysis-based method was employed to quantify changes in fibre Vf, providing insight into the NUFD across the cross-section. The effect of NUFD on compressive strength will be evaluated at both the material and structural levels.

2. Experimental methodology

2.1. Controlled sample manufacturing

The FRP pultruded hollow box profile in this study was manufactured by Wagners Composite Fibre Technology (WCFT) using pull-winding technology [34,35]. The specimens consist of a series of UD and off-axis E-glass fibre plies with a density of 2.54 g/cm^3. These fibres were impregnated with vinyl ester resin through an injection die. The geometric and cross-sectional details of the profile are provided in Table 1. The 0° direction aligns with the specimen's longitudinal axis (pulling direction), and the fibre content in the 0° direction constitutes 78.1% of the total fibre content.

The winding tensions were varied by controlling the yarn path with the steel pins, resulting in different initial thicknesses of the dry preform and NUFDs of the profiles. Fig. 1(b) shows three different yarn paths, representing low, medium and high winding tensions of 2.2 N, 15.3 N and 48.3 N, respectively. The fibre tension values were measured using a

Table 1
Specifications of the hollow box PFRP profiles.

Geometry			Properties		
Wall width (mm)	Wall thickness (mm)	Length (mm)	Fibre content (%)	Fibre volume fraction (%)	Stacking sequence
125	6.4	90/540	0°: 78.1 50°: 21.9	62.5	0/+50/0/-50/0/-50/0/+50/0

Table 2
Winding tension setups as illustrated in Fig. 1(b).

Samples Label	Winder 1	Winder 2	Winder 3	Winder 4
	2nd ply/+50°	4th ply/-50°	6th Layer/-50°	8th Layer/+50°
Low	Low	Low	Low	Low
Medium	Medium	Medium	Medium	Medium
High	High	High	High	High
Mixed	Medium	Medium	Medium	High

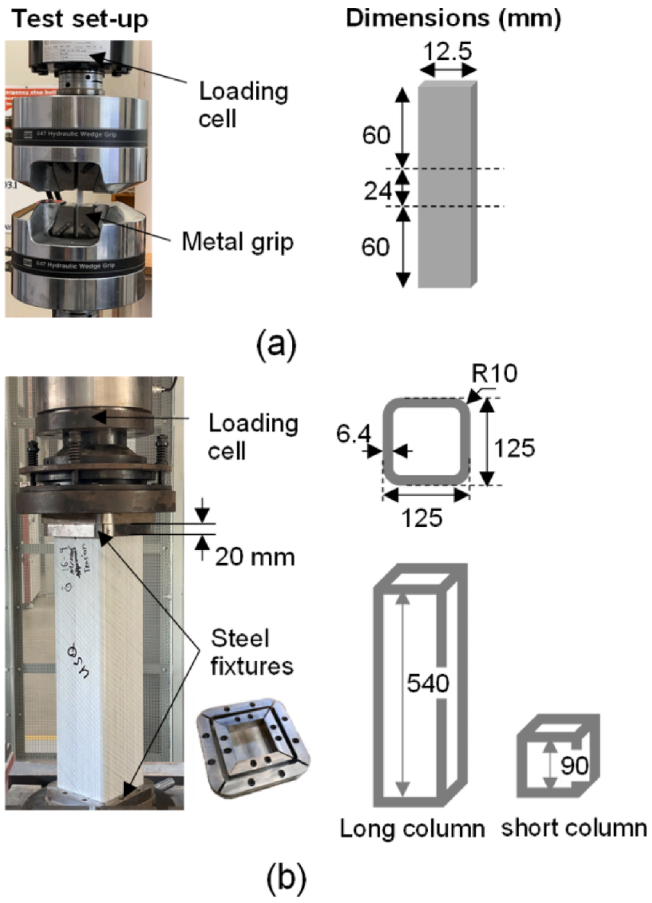

Fig. 2. Schematic of the axis compression test; (a) coupon and (b) PFRP hollow profile.

digital force gauge with a resolution of 0.1 N. Table 2 illustrates the configuration of four winders for four different specimens. Winder 1 lays out the inner off-axis ply, while Winder 4 plies out the outermost off-axis ply in the sequence illustrated in Fig. 1(a).

2.2. Specimen preparation

PFRP profiles were manufactured with four different levels of winding tension: low, medium, high and mixed tension, as shown in Table 2. Coupons and full-scale columns were prepared from the profiles for compression testing. Two groups of coupons were cut using a water-jet machine. One group contained significant NUFD, while the other did not. The columns were categorised into short columns (L90) and long columns (L540), with slenderness ratios of 0.7 and 4.3, respectively. The use of different slenderness ratios for columns allowed for the examination of compressive material failure and buckling failure. The dimensions of these samples are shown in Fig. 2.

A Struers LaboPol equipment was used to grind and polish the specimens for microscopic imaging. The grinding process utilised 1200 and 320 grit papers, followed by a three-step polishing process using DiaPro for 9 μm on an MD-largo plate, DiaPro for 3 μm on an MD-DAC cloth, and OP-U Nondry on a Neoprene cloth. The cross-sections of the samples were then imaged using a Leica DMS300.

2.3. Compression tests

Fig. 2(a) shows the coupon compression test setup using an MTS machine with a 100 kN load cell. The test was conducted at a constant displacement rate of 1 mm/min. Fig. 2(b) depicts the compression test of full-scale PFRP profiles for short and long columns using the SANS machine (SHT4206 – 2000 kN capacity). Steel fixtures were designed to reduce stress concentration and prevent premature failure at the ends. Five specimens were tested in each group to validate the test result and ensure repeatability.

3. Non-uniform fibre distribution formation and characterisation

3.1. Formation of material imperfections

The formation of the NUFD in hollow profiles occurs during the pultrusion process, as shown in Fig. 3(a). During this process, the preform (dry stack) passes through the entry bush into the pultrusion die, where compaction from the die reduces the laminate thickness (Δt). This reduction in thickness leads to excess length in the off-axis plies, resulting in fibre misalignment, in-plane waviness and out-of-plane waviness [25]. The waviness of the off-axis ply occupies the area intended for the UD ply, causing the UD fibres to move laterally and towards low-pressure zones, which results in the formation of NUFD. In extreme cases, the UD ply could be discontinuous and visible on the surface.

The imperfections representing the excess length within the off-axis ply are the in-plane waviness and misalignment, which can be evaluated by the Filtered Canny Misalignment Analysis (FCMA) method [22] based on the image process, as shown in Fig. 3(b). This method calculates the average local fibre angle in relation to the Z-axis and the fibre angle distribution along the X-axis. This ply is divided into three regions, namely zones A, B, and C. The angle distribution forms indicate the presence of fibre waviness in zone A and C and misalignment in zone B. The interface between these zones is always accompanied by significant out-of-plane waviness, as indicated by the red square in Fig. 3(b).

The out-of-plane waviness observed from the cross-section is shown in Fig. 3(c). It has been observed that the severity of out-of-plane waviness in the outer off-axis plies is more significant, as these plies have more excess length compared to the inner plies. As a result, NUFD is mainly observed in the outer UD ply of the composite material.

3.2. Exess length at different winding tension

The excess length in the off-axis plies can be evaluated by measuring the thickness change between the dry preform (t_1) and the final product (t_2), as shown in Fig. 1(c). When the winding angle is 90°, the excess length (L_{ex}) can be calculated by [36]

$$L_{ex} = \frac{2\pi(t_1 - t_2)}{4} \tag{1}$$

It should be highlighted that the final geometry of the PFRP profiles is consistent. Therefore, the excess length of the off-axis ply mainly depends on the initial thickness, which varies with different winding tensions. The initial thickness t_1 can be calculated by the measured diameter of every off-axis ply, and t_2 is measured in the final product.

Fig. 4(a) illustrates the relationship between winding tension and the diameter of each off-axis ply in the composite material. The diameter decreases as the winding tension increases. The outermost wound ply (8th ply) at mixed tension has the same thickness as the high-tension ply, even though the former off-axis layer is different. Fig. 4(b) shows the thickness change of each off-axis ply at different winding tension before and after curing. A lower winding tension leads to greater thickness variation and increased excess length in the off-axis plies. The thickness variability of the outer plies is higher than that of the inner plies, even for off-axis plies with the same winding tension, which is consistent with the observed result in Fig. 3(c).

These thickness variations can contribute to the formation of NUFD in the composite material. Different winding tensions can lead to different NUFDs in the material, highlighting the importance of process optimisation in industrial manufacturing. Furthermore, although the

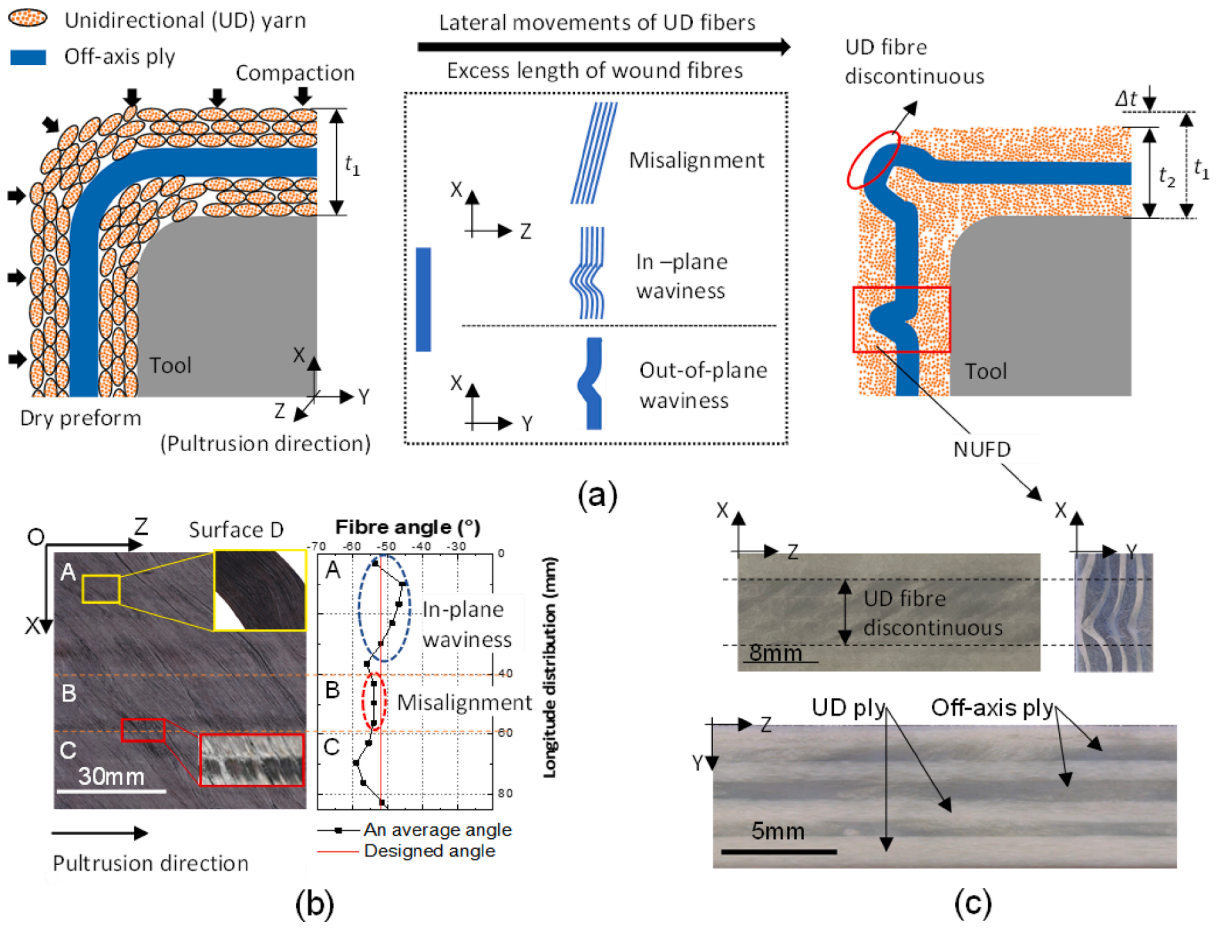

Fig. 3. The formation of the NUFD; (a) compaction of the preform, (b) defects in the off-axis ply and (c) visible discontinuity on the surface and NUFD of the cross-section.

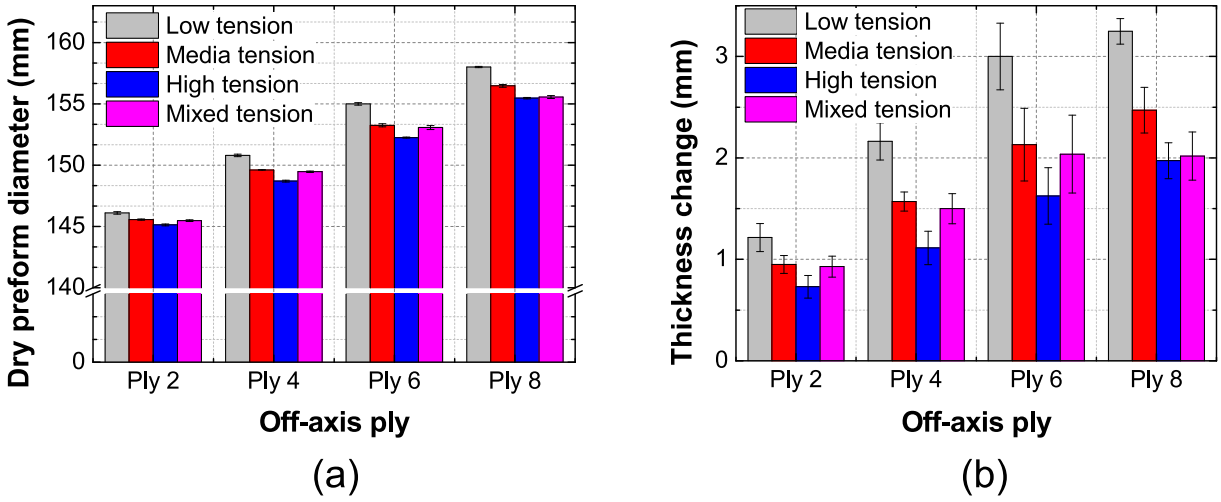

Fig. 4. Thickness change of the off-axis ply; (a) initial outer diameter of each ply and (b) final thickness change for each ply.

high-tension samples have the smallest thickness change, they can increase the pulling force and resin injection pressure during manufacturing. These factors should be considered comprehensively to achieve optimal performance and production efficiency in composite structures. Mixed tension is a balanced approach that can help to mitigate material imperfections and reduce the risk of increasing the pulling force excessively during manufacturing.

3.3. *Measured volume fraction of unidirectional ply*

In this study, NUFD in composite material was quantified using the change in an area of the UD ply. The content ratio of UD and wound fibre is 3.6, and each UD ply consists of three layers of UD yarn in the fibre delivery process, while the off-axis ply only has one layer. This means the thickness change of the off-axis ply can be negligible compared to

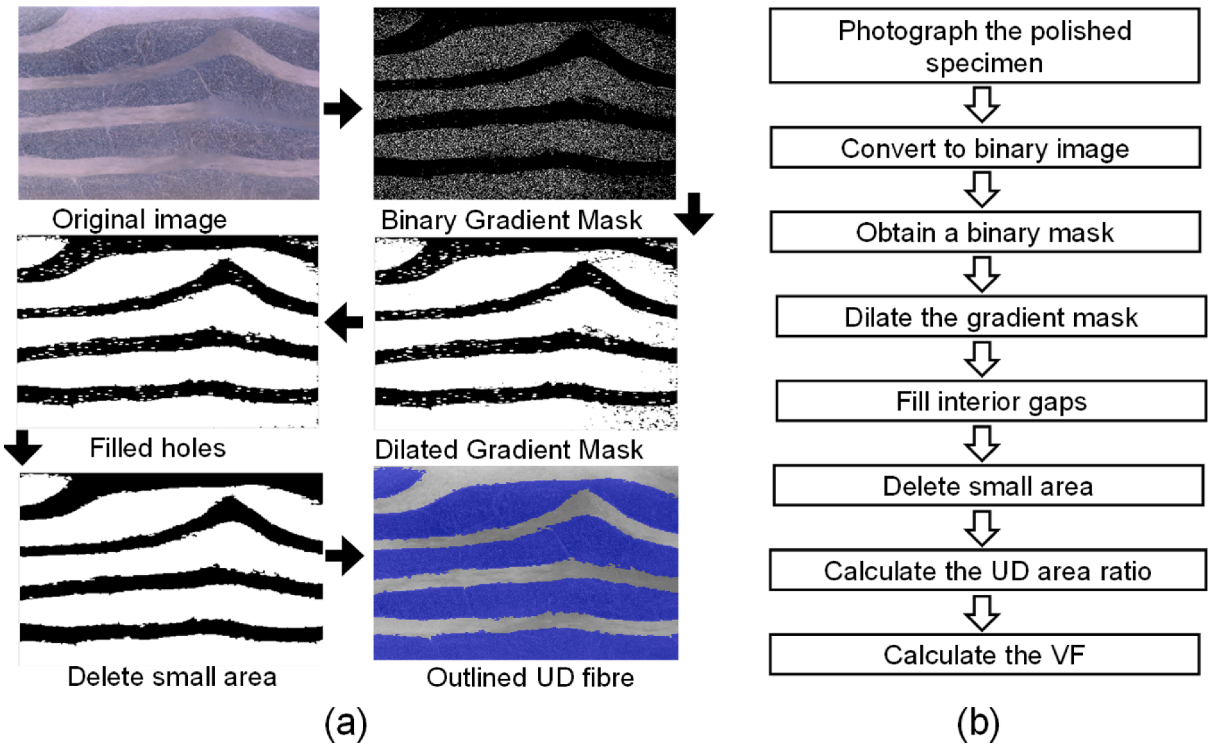

Fig. 5. Segment of UD ply; (a) image analysis and (b) process to calculate the Vf. (For interpretation of the references to colour in this figure legend, the reader is referred to the web version of this article.)

that of the UD ply. When the preform is compacted, the fibres fill the gap between the UD yarn. The UD fibres in the UD ply are assumed to be uniformly distributed for the high Vf. Due to the low volume fibre fraction in the off-axis ply, the residual resin is primarily maintained in the off-axis ply, as shown in the XZ plane of Fig. 3(c). The resin in the UD ply can be neglected compared to the off-axis ply. Therefore, the area of

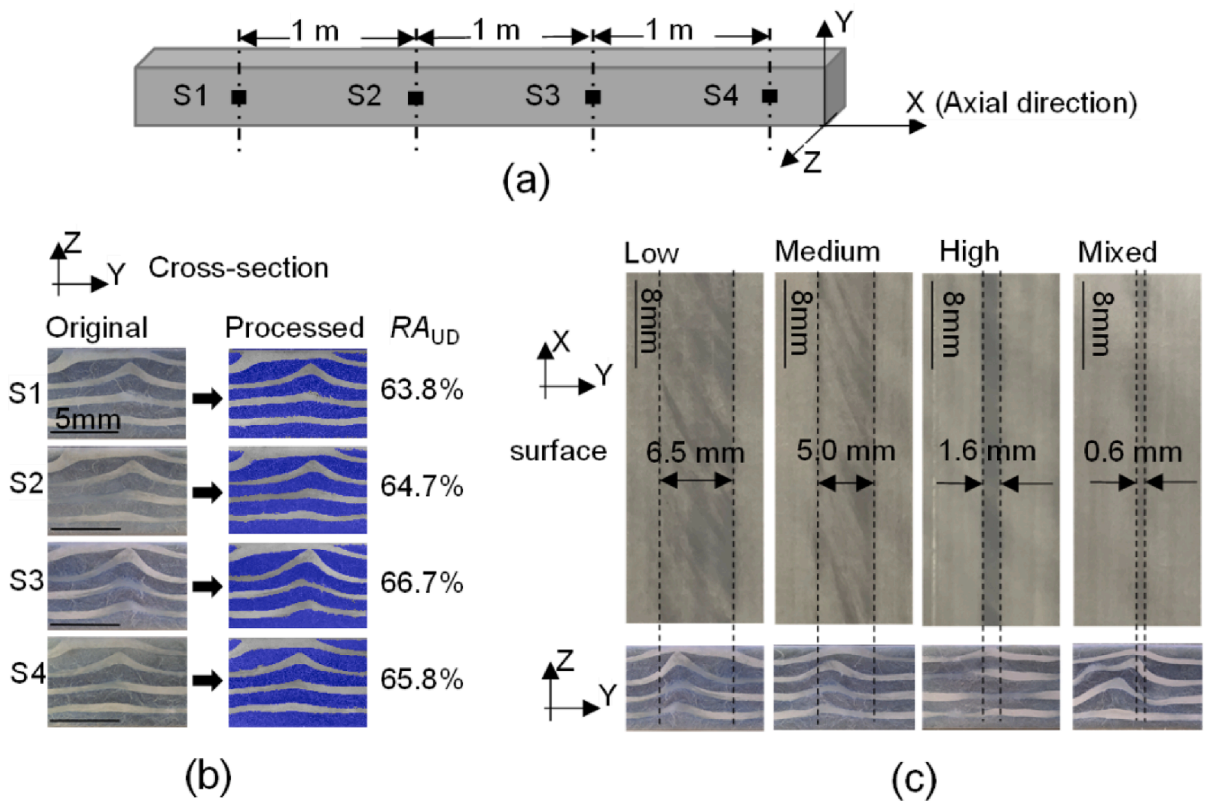

Fig. 6. The defect consistency along the profile axial direction; (a) cutting planes and (b) identified UD ply and the area ratio and (c) effect of winding tension on the top surface and cross-section of the defective coupon.

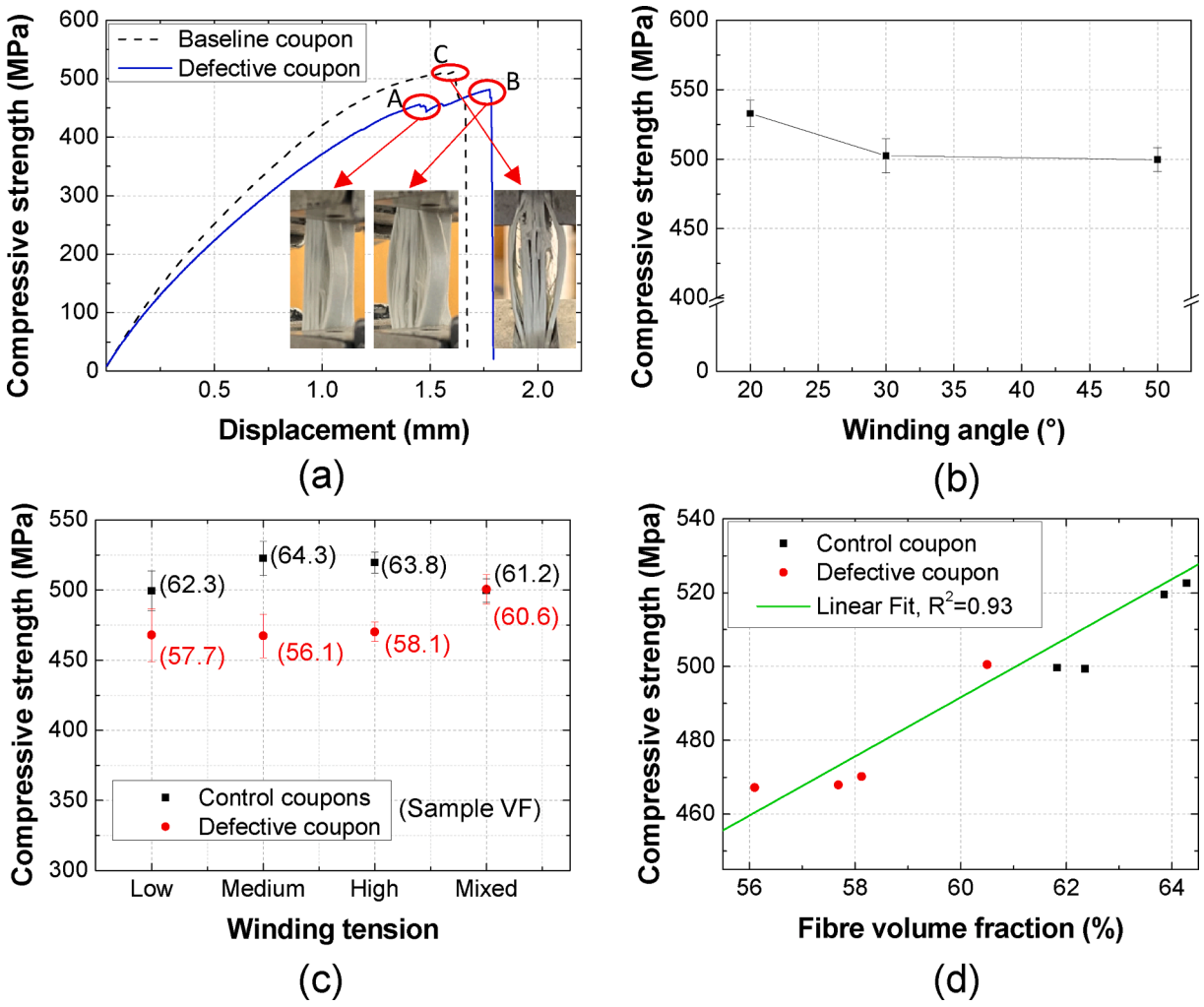

Fig. 7. Material compressive strength of coupons; (a) A typical stress-displacement curve and failure mode of the coupon with and without defects, (b) effect of winding angles, (c) effect of winding tension and (d) effect of fibre Vf.

the UD ply serves the same purpose as the UD fibre Vf in describing the NUFD along the cross-section.

The process of identifying the UD ply in the cross-section of PFRP was carried out using image analysis, which was implemented using MATLAB 2019b. The image of the cross-section was divided into small slices to reflect local Vf over the entire section. Fig. 5 shows the step for analysing one slice. This strategy was based on sufficient contrast of UD and wound plies.

The image was first converted to a greyscale image, and a threshold was used to obtain a binary mask that contains the segmented UD ply. The image was then dilated using a built-in function to reduce the gap in the lines. The residual holes in the UD ply were then filled using 'imfill' function. Then, a complement image was created to eliminate misidentified areas in the wound ply. The segment detected in the previous step in the wound ply will become the holes in the complement image. The holes in the complement image were then filled again. After the misidentified areas were eliminated, the complement image was reversed. The UD ply was marked as green areas in Fig. 5(a). The code is supplied as supplementary material to this paper.

The samples produced through the pull-winding delivery process maintain a consistent total number of UD and wound tows across different winding tensions, resulting in uniform fibre Vf of different profiles. This fibre Vf for each sample is measured by conducting a burn-out test in accordance with ISO 1172 (Table 1). This value serves as the basic fibre Vf (V_{Basic}) for the entire cross-section area. It should be noticed that UD ply and off-axis ply have the same fibre Vf in this profile, according to the product sheet. When ignoring the variation in the gap between fibres in the UD ply, the fibre Vf of *i*th slice V_i can be estimated as follows:

$$V_i = (1+\alpha)V_{Basic} \tag{2}$$

The coefficient α is the rate of change in the proportion of identified UD ply area compared to the average proportion of UD ply area in the cross-section.

The uniformity of the defects along the pultrusion direction is indicated by the stability of the UD ply's cross-section area of the profile. Fig. 6(a) shows that four sections were selected at one-metre intervals along the pultrusion direction. The local cross-sections with UD fibre missing were chosen to show the UD ply distribution, as shown in Fig. 6 (b). Each slice has identical defects with out-of-plane waviness of off-axis ply and UD fibre discontinuity. The ratio of UD ply's cross-sectional area to the total area (RA_{UD}) is consistent with a standard deviation of 1.3%. The uniformity of the defects along the pultrusion direction is indicated by the stability of the UD ply's cross-section area of the profile. This demonstrates the stability of NUFD along the pultrusion direction, with no observed significant out-of-plane waviness in the UD ply and only lateral movement.

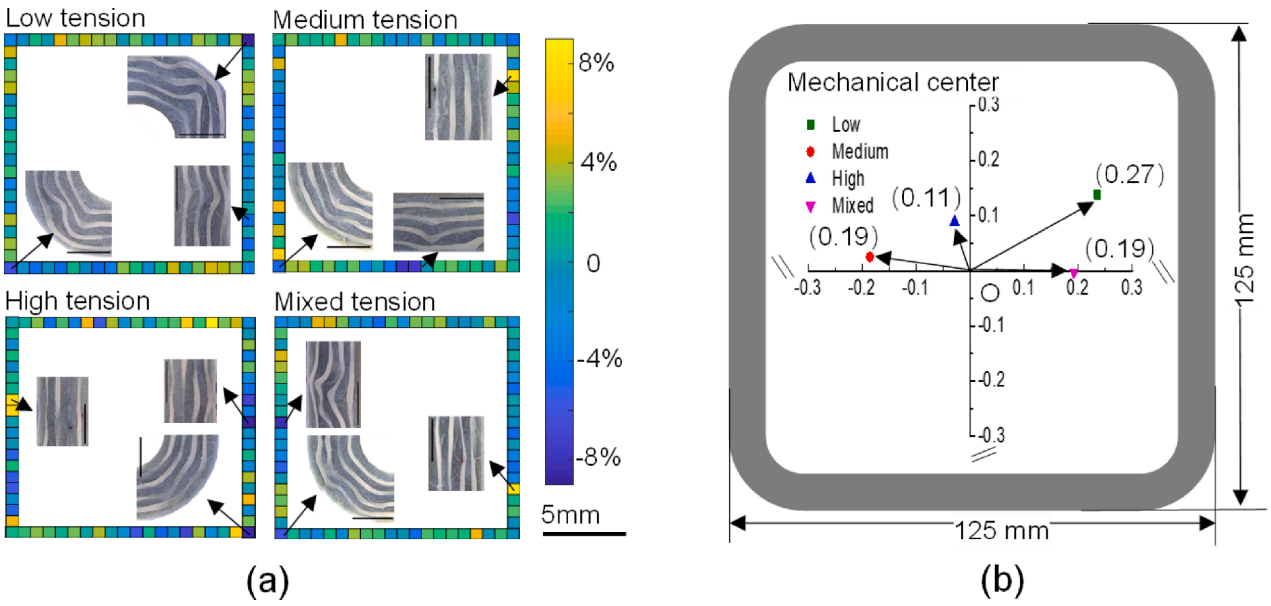

Fig. 8. Experiment measurement of (a) relative fibre Vf deviations (R_i) of the UD ply of PFRP sections and (b) its mechanical centre and eccentric distance.

4. Results and discussion

4.1. Effect of non-uniform fibre distribution on material compressive behaviour

The defective coupon in this research is defined as a discontinuity in the outermost UD ply caused by the out-of-plane waviness of the off-axis ply. This can be seen as a visible imperfection in the top surface and cross-section of the coupon, as shown in Fig. 6(c). The most extensive discontinuous piece, found in the columns at four-winding tensions, is selected as a test coupon. The discontinuous length has been marked on the top surface, as shown in Fig. 6(c). The mixed-tension samples have the least discontinuity, while the low-tension samples have the most. For comparison, baseline samples are randomly selected from the columns without significant waviness and discontinuity.

4.1.1. Effect of non-uniform fibre distribution on failure mode

The presence of NUFD in a coupon leads to early initiation of failure, particularly if there is a fibre discontinuity. This early failure initiation was observed during the experiment in the defective coupons, as shown in Fig. 7(a). The displacement-stress curve was interrupted at point A with an audible crack, resulting in a 2.5% drop in stress and a continued increase. The initial failure occurred due to partial delamination in the outermost ply, where the UD fibres were missing. However, the baseline sample exhibited a brittle behaviour until the final fracture. The final failure mode can be characterised as a fibre fraction and delamination combination.

4.1.2. Effect of non-uniform fibre distribution on compressive strength

The off-axis ply provides increased lateral strength to the profiles [37]. Three profiles were manufactured with three different winding angles (20°, 30° and 50°) to examine the impact of the winding angle on compressive strength. Fig. 7(b) showed that a winding angle of 20° resulted in a 6% increase in compressive strength compared to a 50° winding angle. However, the effect of off-axis ply on longitudinal compression strength was negligible for winding angles above 30°, which is consistent with previous findings [38]. The winding angle in this study was designed to be 50°, so it can be concluded that the in-plane waviness of the off-axis ply did not affect the compressive strength of the coupon test, and any changes in compressive strength were due to the UD fibre alone.

The results of the defective coupon test indicated that NUFD has a significant impact on compressive strength. As seen in Fig. 7(c), the compressive strength of the defective coupons was reduced by up to 11%. The lowest reduction in compressive strength was observed in the mixed-tension coupons, which had smaller discontinuities, 0.6 mm versus 6.5 mm, in the UD fibre compared to the lowest tension coupons. These results highlight the importance of controlling NUFD in the pultrusion process to maintain the mechanical properties of the composite material.

The discontinuity length presented in Fig. 6(c) takes into account the outermost ply, which is an extreme case of NUFD. On the other hand, the Vf of the coupon can also reflect the distribution of other UD plies. The results in Fig. 7(c) show that the trend of the Vf is consistent with the trend in compressive strength for various tension coupons. A Pearson correlation coefficient of 0.96 was obtained, which indicates a linear relationship between the UD ply and compressive strength, as shown in Fig. 7(d). This finding is in agreement with [39].

Table 3
The ratio of the cross-sectional area of the UD plies to the total cross-sectional area.

Samples	Wall (%)					Corner (%)		Whole (%)
	Top	Bottom	Left	Right	Dev.	Average	Dev.	Average
Low	73.9 (1.6)	73.7 (1.7)	73.2 (2.3)	72.5 (2.0)	5.1	69.1 (2.1)	9.1	72.91(2.32)
Medium	72.7 (1.4)	71.8 (2.6)	72.3 (2.6)	72.2 (2.4)	7.7	70.7 (2.3)	5.0	72.12(2.31)
High	73.4 (2.8)	72.2 (3.0)	72.4 (2.6)	71.3 (3.2)	11.2	70.4 (3.1)	8.6	72.14(2.97)
Mixed	73.3 (1.9)	73.0 (2.5)	73.4 (1.7)	72.3 (2.3)	8.5	70.7 (1.6)	5.9	72.78(2.17)

*The number between parenthesis is the standard deviation.

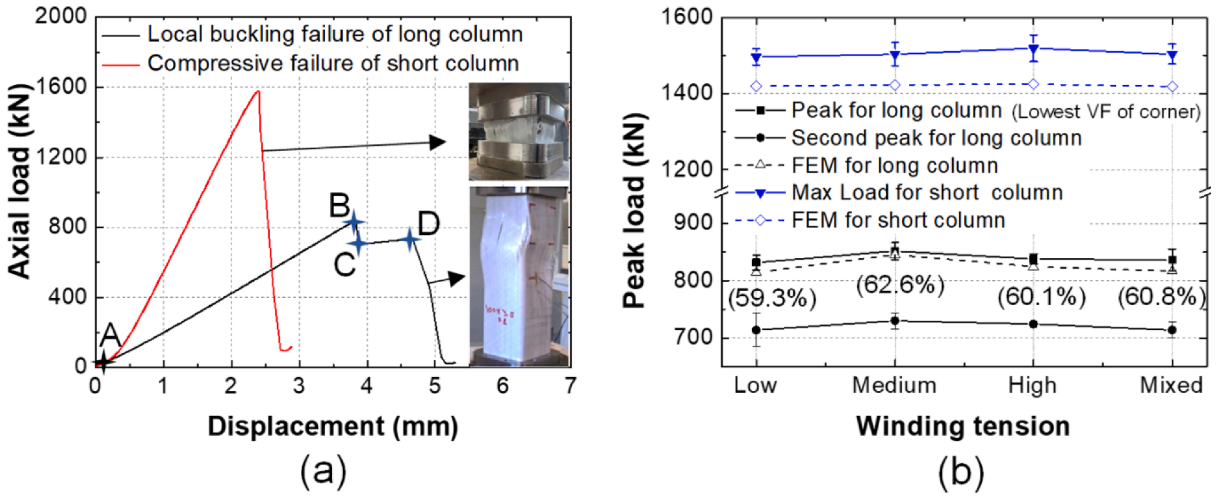

Fig. 9. Axial compression of short columns L91 and long columns L540; (a) load–displacement curves and (b) maximum peak loads, including numerical predictions and second peak loads.

4.2. Effect of non-uniform distribution on structural compressive behaviour

4.2.1. Characterisation of unidirectional fibre distribution across the section

The image analysis method is used to determine the fibre Vf across the entire cross-section. Fig. 8(a) shows 76 evenly-spaced sampling locations. Table 3 shows the ratio of the cross-sectional area of the UD ply to the total cross-sectional area for each location. The average cross-sectional area of the UD ply across all sections is similar, indicating that winding tension has no effect on the total cross-sectional area of the UD ply. This aligns with the volume of UD fibres used in the pull-winding delivery system at different winding tension manufacturing. The results demonstrate that the image analysis method effectively characterises the distribution of fibre volume across the cross-section, and its accuracy is supported by reasonable assumptions, as discussed in Section 3.3. The related cross-sectional area of the UD ply is then converted to fibre Vf using Eq. (2). The ratio of unidirectional fibres at the corner is lower compared to wall fibres, suggesting that the corner is more susceptible to NUFD.

The relative deviation of fibre Vf (R) is used to analyse the distribution of the UD ply across the PFRP cross-section through

$$R_i = \frac{V_i - V_{Basic}}{V_{Basic}} \tag{3}$$

Where R_i is the relative deviation of the Vf of ith sampling location; V_i is the calculated Vf at ith sampling location; and V_{Basic} is the average Vf of the PFRP cross-section. A negative R_i indicates that this region is probably impacted by the out-of-plane waviness of the off-axis ply, leading to the NUFD of the UD ply. The positive R_i indicates that the lateral moved UD fibres are filling the yarn space in off-axis plies. Zero means that there is a uniform distribution in this area.

Fig. 8(a) shows the relative distribution of UD fibre and its features at the extreme points for samples under different winding tensions. The results indicate the presence of the NUFD. It can be observed that the corners, particularly for the low-tension sample, are susceptible to out-of-plane waviness and discontinuity of the UD ply, resulting in a reduced fibre Vf. The accumulation of excess length is more prone to occur at the corner during the compaction of the preform [36]. The Vf of UD fibres increases near the corners as the UD fibres shift away from the corner. The low-tension sample shows the highest deviation at the corner, which is 9.1%, according to Table 3. On the other hand, the high-tension sample exhibits the highest deviation on the wall, which is around 11.2%.

Low-tension samples experience the greatest thickness change in the off-axis ply, resulting in the most severe UD ply discontinuity in the outermost ply and the lowest fibre Vf at the corner. High-tension samples have less severe out-of-plane waviness in the off-axis ply due to lower thickness changes (the lower initial excess length prior to compaction), as discussed in Section 3. The movement of UD fibres in high-tension is smoother than in low-tension samples. Mixed tension samples have less excess length in the outermost off-axis ply due to its high winding tension, but the inner plies exhibit out-of-plane waviness at the regions of minimal fibre Vf. The causes and manifestations of NUFD depend on the winding tension.

NUFD will increase the eccentricity of the cross-section, which is a factor in reducing the buckling load under axial compression. Fig. 8(b) shows the calculated mechanical centre and eccentric distance based on the fibre Vf distribution along the cross-section. The maximum eccentricity was observed in the sample with low winding tension, with an eccentric distance of 0.27 mm and a normalised value of 0.008 relative to the radius of gyration. As a comparison, the relative eccentric distance for the box section in [10] is 0.012, and the resistance reduction factor is 0.93 when the slenderness ratio is 70.

4.2.2. Compressive strength of columns

The load–displacement behaviour of columns with different slenderness ratios is depicted in Fig. 9(a). The considered ratios are 0.7 and 4.3, which result in compressive material failure and significant local buckling, respectively. The load–displacement curve for the short column exhibits a catastrophic failure, while the curve for the long column exhibits a progressive failure. The slope of the linear curve represents the axial stiffness of the column and varies with the column length. For the long column, a sudden drop in axial load resistance occurs between points B and C after the linear relationship, accompanied by local buckling in the walls. This decline from point B to C is around 12%. There is a delay between points C and D, indicating progressive failure due to the role of the wound fibre [40]. The load–displacement curve trend is similar for different winding tension samples.

Fig. 9(b) shows the experimental and numerical results for the axial compression of short columns L90 and long columns L540. For the short column, there is no significant variance in the maximum load both from experiments and numerical. For the long columns, the samples with medium tension have the highest peak load than others. Moreover, the samples with medium tension have the highest fibre Vf at the corner. The analysis of variance (ANOVA) was used to analyse differences in groups, and the calculated probability (P-value) for the maximum and second peak load was found to be 0.282 and 0.491, respectively, which is higher than the significance level (0.05). The null hypothesis is

Table 4
Elastic properties of fibre and matrix and strength limits and fracture energy values of the pultruded lamina.

Property	Description	Symbol	Value
Fibre	Young's elastic modulus/GPa	E_f	73
	Shear elastic modulus/GPa	G_f	30
	Poisson's ratio	υ_f	0.22
Matrix	Young's elastic modulus/GPa	E_m	3.4
	Shear elastic modulus/GPa	G_m	1.3
	Poisson's ratio	υ_m	0.35
Lamina strength limits (MPa)	Longitudinal tensile strength/	X^T	803
	Longitudinal compressive strength	X^C	548
	Transverse tensile strength	Y^T	43
	Transverse compressive strength	Y^C	187
	Longitudinal Shear strength	S^L	64
	Transverse Shear strength	S^T	50
Lamina fracture energy (N/mm)	Longitudinal tensile fracture energy	G_{LT}	92
	Longitudinal compressive fracture energy	G_{LC}	79
	Transverse tensile fracture energy	G_{TT}	5
	Transverse compressive fracture energy	G_{TC}	5

accepted, indicating that there is no significant difference between groups. A trend can still be found in which the maximum axial load is correlated with the lowest fibre Vf at the corner, although the variation between the samples at the corner is only about 3%. These samples in this research were optimised for industrial use, and the manufacturing process only took into account the effect of winding tension. Lower fibre Vf may be present in other pultruded composite profiles [7]. These findings will be further discussed in Section 5 using the FE model, including the analysis of worse cases and sensitive analysis of NUFD.

5. Finite element analysis of the composites with defects

5.1. Finite element modelling

Abaqus/CAE 2019 was employed to investigate the influence of the NUFD on the axial compression behaviour of composite structures. The explicit dynamic solver with the Hashin damage model was implemented to capture local buckling and prevent convergence issues. The FE analysis used 8-node quadrilateral general-purpose continuum shells (SC8R) with a mesh size of 5 mm and six elements through thickness. The strength limits and fracture energy values for the Hashin model are presented in Table 4 [41].

As shown in Fig. 10(a), the FE model accounts for the variation in fibre Vf by using a predefined field in Abaqus. The fibre Vf for each element is defined based on its coordinates. The fibre Vf remains consistent along the pultrusion direction due to the uniformity of the defects in this direction, as discussed in Section 3.3. This observation for pultruded profile is also supported by reference [7]. The properties of the fibre and resin are listed in Table 4 and obtained from [7,42]. The elastic modulus E_{11}, E_{22} and shear modulus G_{12}, G_{23} were calculated using the rule of mixture [5,43].

The results of the FE model show a good agreement with the experimental data. Fig. 10(c) shows the FE result of load–displacement curves for the low winding tension sample, which are consistent with the experimental results. The other three cases are depicted in Appendix A.

The Hashin damage initiation criteria for fibre compression (HSNFCCRT) is used to track the waviness extent, while the transverse shear damage in the matrix (DAMAGESHR) serves as an indication of delamination propagation. These criteria facilitate the tracking of the

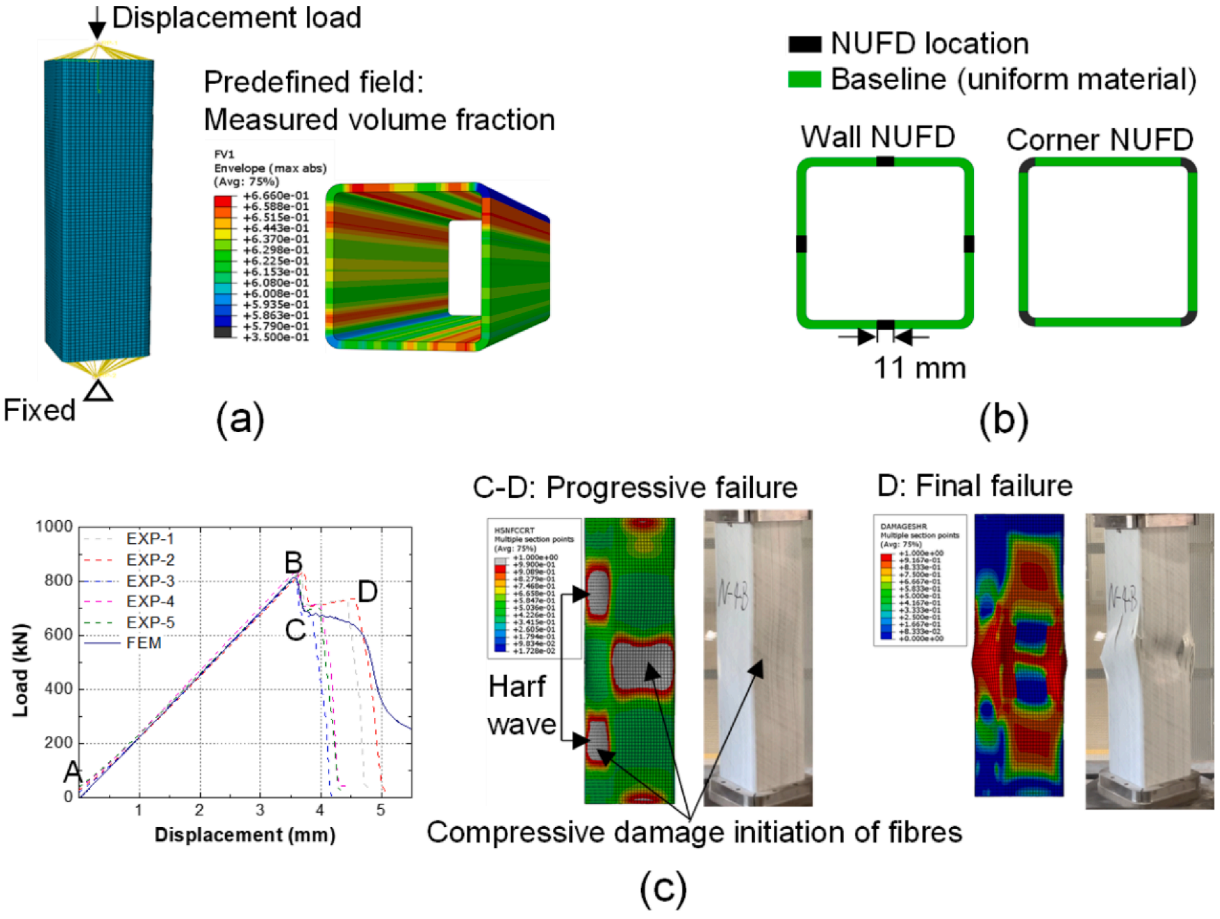

Fig. 10. (a) FE modelling of the pultruded column with NUFD, (b) defects position and (c) numerical and experimental load–displacement curves and the failure modes.

Table 5
Effect of the non-uniform fibre distribution on experimental and predicted compression strength of short columns and long columns.

Fibre distribution		Peak load- short columns L90 (kN)					Peak load- long columns L540 (kN)				
		FE model		Experiment			FE model		Experiment		
		No-Hasin	Hashin	Ave.	St.D.	COV(%)	Elastic	Hashin	Ave.	St.D.	COV(%)
Uniform		3494.2	1433.1	–	–	–	857.5	862.8	–	–	–
Non-uniform	Low	3103.2	1420.1	1496.5	21.0	1.4	813.4	817.2	832.1	12.9	1.5
	Medium	3124.2	1423.2	1503.5	30.2	2.0	849.5	850.0	851.8	14.8	1.7
	High	3053.5	1425.1	1519.2	35.1	2.3	825.4	827.5	838.0	8.9	1.1
	Mixed	3049.3	1418.9	1503.6	26.0	1.7	820.4	820.6	836.2	19.1	2.3

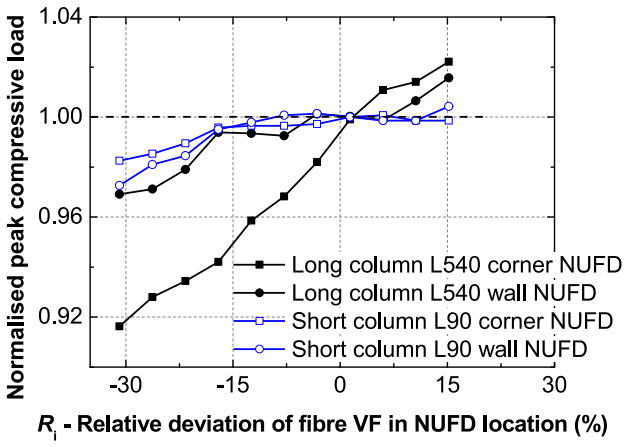

Fig. 11. Numerical analysis of defect sensitivity on the compressive peak load for the short columns L90 and the long columns L540.

respective failure modes, as described in reference [40]. Fig. 10(c) shows that this FE model can accurately capture the failure mode in comparison to the experimentally observed failure mode. The FE analysis results for buckling load under different winding tensions present the same trend as the experimental findings, even though the variation of the fibre Vf is 3%, as shown in Fig. 9(b). These results demonstrate that this FE model is reliable in predicting the buckling load of composites under axial compression.

5.2. Defect sensitivity analysis

The failure modes observed experimentally in the hollow column samples include compressive material failure for short column L90 and local buckling failure for long column L540, as shown in Fig. 9(a). The peak load in the simplified FE model without Hashin damage definition corresponds to the local structural buckling, as the material failure is suppressed. This provides a reference point to determine the failure mode when the Hashin damage is implemented. When both models predict the same peak load, the failure mode is local buckling. Otherwise, the failure mode is a compressive material failure.

Table 5 shows the comparison of these two models for the short

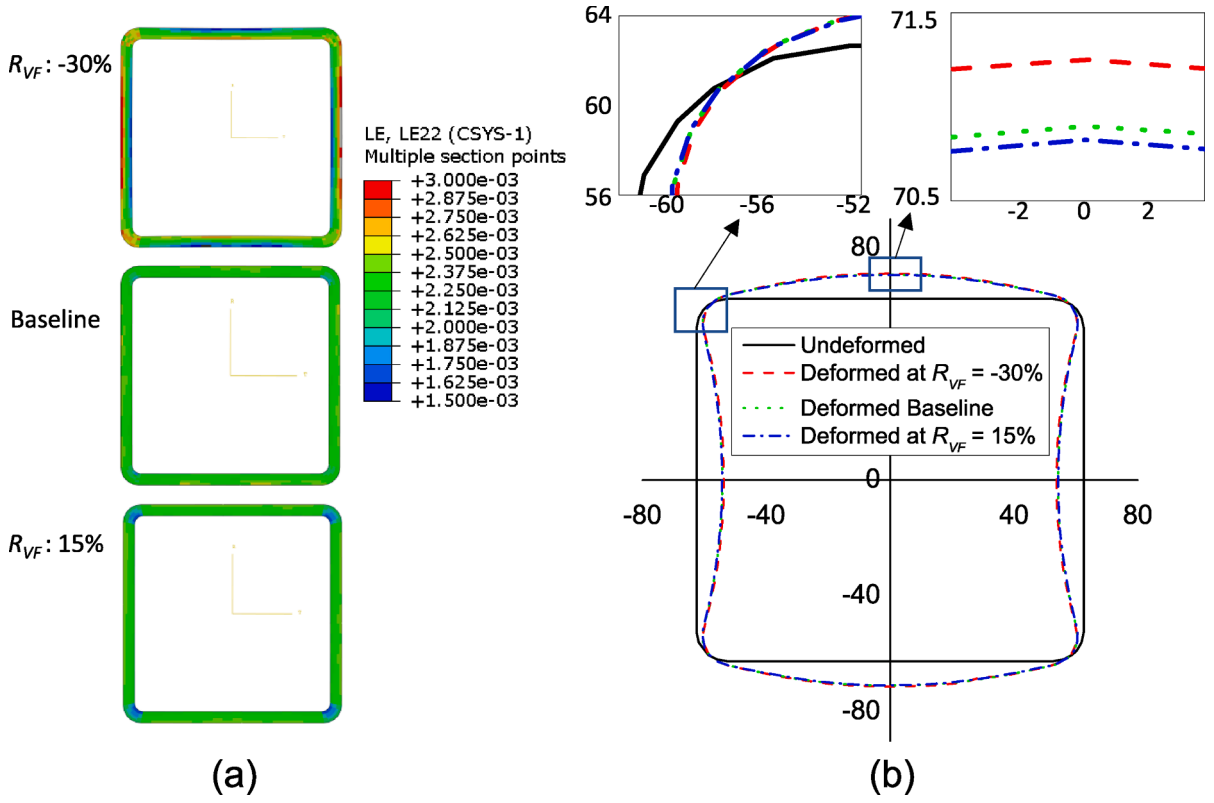

Fig. 12. Effects of corner NUFD on compressive response in the middle cross-section of the long columns L540 with corner defect; (a) logarithmic strain distribution and (b) deformation.

columns and long columns. For the short columns, the material has reached the limitation before the load capacity reaches the local buckling load from the FEM result, which is in accordance with the experimental result. For the long columns, the predicted peak values for the two models are equal, indicating that the failure is local structural buckling, as shown in Fig. 10(c).

The cross-sectional location of NUFD was a key factor in compressive performance experimentally. For example, the test samples with the medium tension have the highest peak load, of which the localised fibre Vf at the corner is the highest. In order to examine the relationship between the NUFD location and peak load, corner NUFD and wall NUFD are investigated separately. The NUFD locations in the FE model are shown in Fig. 10(b) and are marked in black. The NUFD is formed by changing the local fibre Vf in comparison to the adjacent area. The wall NUFD is 11 mm long, which has the same cross-sectional area as the corner NUFD. The baseline fibre Vf in the cross-section was 62.5%, while the relative deviation of fibre Vf in the NUFD area varies between −31% and 15%. The max load of the non-uniform material model is normalised by the max load from the baseline model ($R_{Vf} = 0$).

Fig. 11 shows the effect of the NUFD location on compressive material failure (short columns L90) and local buckling failure (long columns L540). For short column L90, NUFD location on both corners and walls has a limited effect on load capacity, which is consistent with previous findings [44]. The peak load reduction is 2% for corner NUFD and 3% for wall NUFD when the fibre Vf decreases by 30%. However, for long columns L540 with local buckling, the corner NUFD reduces the peak load by 9%, while the wall NUFD reduces the peak load by 3% when the local fibre Vf decreases by 30%. The results indicate that corner NUFD is a significant defect, as the majority of structural applications are considered as long columns and governed by local buckling failure. Furthermore, there is a linear relationship between the relative deviation of the local fibre Vf and the peak reduction factor.

The effect of corner NUFD on resistance to buckling load in hollow profiles can be assessed by the rotation stiffness of the corner [45]. A change in the fibre Vf at the corner resulted in a variation in the corner rotation stiffness. As shown in Fig. 12(a), there is a change in logarithmic strain with the fibre Vf at the corner in the tangential direction of the cylindrical coordinate at the same loading displacement point. It can be observed that the strain along the cross-section decreases with an increase in the fibre Vf due to the higher corner rotation stiffness. This observation aligns with the findings reported in the reference [46], which suggest that increasing the corner area can effectively reduce stress concentration. When local buckling occurs in the column, the deformation of the local buckling plane can be observed in Fig. 12(b). The lower corner fibre Vf leads to a larger displacement at the buckling plane. The results indicate that the rotation stiffness at the corner plays an important role in local buckling in the hollow profiles, which is consistent with the plate theory [47].

6. Conclusions

This paper investigates the formation of Non-uniform Fibre Distribution (NUFD) in Pultruded Fibre Reinforced Polymer (PFRP) and its effects on the material and structural behaviour under axial compression. The following conclusions are drawn from the study.

- The excess length of the off-axis layer generates fibre waviness due to compaction through the pultrusion die, leading to the formation of NUFD in the cross-section. A MATLAB-based image analysis was developed to measure the localised fibre Vf variation. Results show that the samples with the lowest winding tension exhibit the largest reduction in fibre content, with a decrease of up to 9% at the corner. In addition, the fibre distribution remains consistent along the axial pultrusion direction.
- The influence of the NUFD on the material compressive strength was investigated by testing coupons with visible surface fibre discontinuities. Results showed that fibre discontinuities had a negative effect on material strength under axial compression. Specifically, when the fibre Vf decreased by 12%, the load capacity of the coupon decreased by 11%.
- A FE model with measured localised fibre Vf was developed to evaluate the effect of the NUFD on compressive material failure and local buckling failure in short columns and long columns. The NUFD has a limited effect on the load-bearing capacity of short columns. However, for the corner NUFD in long columns, the reduction peak load is significant, up to 9%. The modelling highlights that the variation in rotational stiffness at the corner is crucial to the local buckling load capacity of hollow composite columns.

CRediT authorship contribution statement

Songming Qi: Conceptualization, Methodology, Software, Investigation, Writing – original draft, Writing – review & editing. **Omar Alajarmeh:** Formal analysis, Methodology, Writing – review & editing. **Tristan Shelley:** Methodology, Writing – review & editing. **Peter Schubel:** Supervision, Writing – review & editing. **Kendric Rendle-Short:** Formal analysis, Investigation, Resources. **Xuesen Zeng:** Supervision, Conceptualization, Methodology, Writing – review & editing.

Declaration of Competing Interest

The authors declare that they have no known competing financial interests or personal relationships that could have appeared to influence the work reported in this paper.

Data availability

No data was used for the research described in the article.

Acknowledgements

The work was funded through a Cooperative Research Centres Projects (CRC-P) Grant (CRCPSIX000117).

Appendix A. FEM vs experimental load-displacement curves

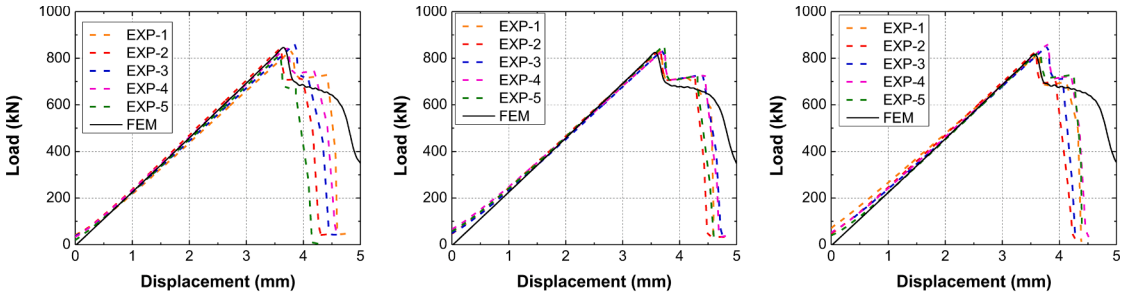

(a) Samples with Medium Tension (b) Samples with High Tension (c) Samples with Mixed Tension

Appendix B. Supplementary data

Supplementary data to this article can be found online at https://doi.org/10.1016/j.compositesa.2023.107659.

References

[1] Guades E, Aravinthan T, Islam M, Manalo A. A review on the driving performance of FRP composite piles. Compos Struct 2012;94(6):1932–42.
[2] Hollaway L. A review of the present and future utilisation of FRP composites in the civil infrastructure with reference to their important in-service properties. Constr Build Mater 2010;24(12):2419–45.
[3] Hassan MH, Othman AR, Kamaruddin S. A review on the manufacturing defects of complex-shaped laminate in aircraft composite structures. Int J Adv Manuf Technol 2017;91(9):4081–94.
[4] Mahadik Y, Hallett SR. Effect of fabric compaction and yarn waviness on 3D woven composite compressive properties. Compos A Appl Sci Manuf 2011;42(11): 1592–600.
[5] Barbero EJ. Introduction to composite materials design. CRC Press; 2010.
[6] Poulton M, Sebastian W. Taxonomy of fibre mat misalignments in pultruded GFRP bridge decks. Composites Part A: Applied Science and Manufacturing; 2021. p. 142.
[7] Feng P, Wu Y, Liu T. Non-uniform fiber-resin distributions of pultruded GFRP profiles. Composites Part B: Engineering; 2021.
[8] Yuksel O, Sandberg M, Hattel JH, Akkerman R, Baran I. Mesoscale process modeling of a thick pultruded composite with variability in fiber volume fraction. Materials (Basel) 2021;14(13).
[9] Bednarcyk BA, Aboudi J, Arnold SM. The effect of general statistical fiber misalignment on predicted damage initiation in composites. Compos B Eng 2014; 66:97–108.
[10] Potter K, Khan B, Wisnom M, Bell T, Stevens J. Variability, fibre waviness and misalignment in the determination of the properties of composite materials and structures. Compos A Appl Sci Manuf 2008;39(9):1343–54.
[11] Ghayoor H, Marsden CC, Hoa SV, Melro AR. Numerical analysis of resin-rich areas and their effects on failure initiation of composites. Compos A Appl Sci Manuf 2019;117:125–33.
[12] Safonov A, Gusev M, Saratov A, Konstantinov A, Sergeichev I, Konev S, et al. Modeling of cracking during pultrusion of large-size profiles. Compos Struct 2020; 235:111801.
[13] Ascione L, Berardi VP, Giordano A, Spadea S. Pre-buckling imperfection sensitivity of pultruded FRP profiles. Compos B Eng 2015;72:206–12.
[14] Baran I, Straumit I, Shishkina O, Lomov SV. X-ray computed tomography characterization of manufacturing induced defects in a glass/polyester pultruded profile. Compos Struct 2018;195:74–82.
[15] Mehdikhani M, Breite C, Swolfs Y, Wevers M, Lomov SV, Gorbatikh L. Combining digital image correlation with X-ray computed tomography for characterization of fiber orientation in unidirectional composites. Composites Part A: Applied Science and Manufacturing; 2021. p. 142.
[16] Nguyen NQ, Mehdikhani M, Straumit I, Gorbatikh L, Lessard L, Lomov SV. Micro-CT measurement of fibre misalignment: Application to carbon/epoxy laminates manufactured in autoclave and by vacuum assisted resin transfer moulding. Compos A Appl Sci Manuf 2018;104:14–23.
[17] Qi S, Alajarmeh O, Shelley T, Schubel P, Rendle-Short K, Zeng X. Fibre waviness characterisation and modelling by Filtered Canny Misalignment Analysis (FCMA). Compos Struct 2023;307:116666.
[18] Baran I. Pultrusion: state-of-the-art process models. Smithers Rapra 2015.
[19] Fairuz A, Sapuan S, Zainudin E, Jaafar C. Polymer composite manufacturing using a pultrusion process: A review. Am J Appl Sci 2014;11(10):1798.
[20] Ramôa Correia J. 9 - Pultrusion of advanced fibre-reinforced polymer (FRP) composites. In: Bai J, editor. Advanced Fibre-Reinforced Polymer (FRP) Composites for Structural Applications: Woodhead Publishing; 2013. p. 207-51.
[21] Struzziero G, Maistros GM, Hartley J, Skordos AA. Materials modelling and process simulation of the pultrusion of curved parts. Compos A Appl Sci Manuf 2021;144: 106328.
[22] Alajarmeh O, Zeng X, Aravinthan T, Shelley T, Alhawamdeh M, Mohammed A, et al. Compressive behaviour of hollow box pultruded FRP columns with continuous-wound fibres. Thin-Walled Struct 2021;168:108300.
[23] Mindermann P, Witt M-U, Gresser GT. Pultrusion-winding: A novel fabrication method for coreless wound fiber-reinforced thermoset composites with distinct cross-section. Compos A Appl Sci Manuf 2022;154:106763.
[24] Sandberg M, Yuksel O, Baran I, Hattel JH, Spangenberg J. Numerical and experimental analysis of resin-flow, heat-transfer, and cure in a resin-injection pultrusion process. Compos A Appl Sci Manuf 2021;143:106231.
[25] Lightfoot JS, Wisnom MR, Potter K. A new mechanism for the formation of ply wrinkles due to shear between plies. Compos A Appl Sci Manuf 2013;49:139–47.
[26] Hallander P, Akermo M, Mattei C, Petersson M, Nyman T. An experimental study of mechanisms behind wrinkle development during forming of composite laminates. Compos A Appl Sci Manuf 2013;50:54–64.
[27] Nosrat Nezami F, Gereke T, Cherif C. Analyses of interaction mechanisms during forming of multilayer carbon woven fabrics for composite applications. Compos A Appl Sci Manuf 2016;84:406–16.
[28] Sjölander J, Hallander P, Åkermo M. Forming induced wrinkling of composite laminates: A numerical study on wrinkling mechanisms. Compos A Appl Sci Manuf 2016;81:41–51.
[29] Thompson AJ, Belnoue JPH, Hallett SR. Modelling defect formation in textiles during the double diaphragm forming process. Composites Part B: Engineering; 2020. p. 202.
[30] Naouar N, Vidal-Salle E, Schneider J, Maire E, Boisse P. Meso-scale FE analyses of textile composite reinforcement deformation based on X-ray computed tomography. Compos Struct 2014;116:165–76.
[31] Kulkarni P, Mali KD, Singh S. An overview of the formation of fibre waviness and its effect on the mechanical performance of fibre reinforced polymer composites. Composites Part A: Applied Science and Manufacturing; 2020. p. 137.
[32] Alves MP, Cimini Junior CA, Ha SK. Fiber waviness and its effect on the mechanical performance of fiber reinforced polymer composites: An enhanced review. Composites Part A: Applied Science and Manufacturing; 2021. p. 149.
[33] Carraro P, Maragoni L, Quaresimin M. Influence of manufacturing induced defects on damage initiation and propagation in carbon/epoxy NCF laminates. Adv Manuf Polym Compos Sci 2015;1(1):44–53.
[34] Guades E, Aravinthan T, Islam MM. Characterisation of the mechanical properties of pultruded fibre-reinforced polymer tube. Mater Des 2014;63:305–15.
[35] Al-saadi AU, Aravinthan T, Lokuge W. Effects of fibre orientation and layup on the mechanical properties of the pultruded glass fibre reinforced polymer tubes. Eng Struct 2019;198.
[36] Thompson AJ, McFarlane JR, Belnoue JPH, Hallett SR. Numerical modelling of compaction induced defects in thick 2D textile composites. Mater Des 2020;196.
[37] Haj-Ali R, Kilic H. Nonlinear behavior of pultruded FRP composites. Compos B Eng 2002;33(3):173–91.
[38] Zhang S, Caprani C, Heidarpour A. Influence of fibre orientation on pultruded GFRP material properties. Compos Struct 2018;204:368–77.
[39] Sitohang RDR, Grouve WJB, Warnet LL, Akkerman R. Effect of in-plane fiber waviness defects on the compressive properties of quasi-isotropic thermoplastic composites. Compos Struct 2021;272.
[40] Alhawamdeh M, Alajarmeh O, Aravinthan T, Shelley T, Schubel P, Kemp M, et al. Modelling hollow pultruded FRP profiles under axial compression: Local buckling and progressive failure. Compos Struct 2021;262.

[41] Sharma AP, Khan SH, Parameswaran V. Experimental and numerical investigation on the uni-axial tensile response and failure of fiber metal laminates. Compos B Eng 2017;125:259–74.
[42] Huang W, Causse P, Hu H, Belouettar S, Trochu F. Transverse compaction of 2D glass woven fabrics based on material twins - Part I: Geometric analysis. Compos Struct 2020;237:10.
[43] Huang ZM. Micromechanical strength formulae of unidirectional composites. Mater Lett 1999;40(4):164–9.
[44] Zhang L, Zhang S, Xu D, Chen X. Compressive behavior of unidirectional FRP with spacial fibre waviness and non-uniform fibre packing. Compos Struct 2019;224:111082.
[45] Liu T, Harries KA. Flange local buckling of pultruded GFRP box beams. Compos Struct 2018;189:463–72.
[46] Alhawamdeh M, Alajarmeh O, Aravinthan T, Shelley T, Schubel P, Mohammed A, et al. Design optimisation of hollow box pultruded FRP profiles using mixed integer constrained Genetic algorithm. Compos Struct 2022;302:116247.
[47] Kollár L, Springer G. Thin Plates. In: Springer GS, Kollár LP, editors. Mechanics of Composite Structures. Cambridge: Cambridge University Press; 2003. p. 89–168.